Check for updates

A direct method for phosphorus atom insertion *via* phosphorous acid for synthesizing P-doped curved polycyclic π-systems

Tomohiro Higashino, [ID] *[a] Yoshifumi Nishida,[a] Keiichi Ishida,[a] Shunsuke Kozaka,[b] Yuka Yasuda,[b] Hironori Kaji [ID] [b] and Hiroshi Imahori [ID] *[a,c,d]

The introduction of heteroatoms into π-conjugated frameworks has emerged as a powerful strategy to modulate their electronic and optical properties. Among these, the incorporation of phosphorus atoms imparts electron-accepting character and distinct photophysical behaviors. However, the direct formation of three C–P bonds from inorganic phosphorus sources remains extremely challenging. While Friedel–Crafts-type C–P bond formation using chlorophosphines offers an effective route to P-doped π-conjugated molecules, the direct synthesis of triarylphosphine from inorganic phosphorous compounds through a triple C–P bond formation has been rarely achieved. Recently, triflic anhydride (Tf$_2$O)-mediated C–P bond formation using organophosphorus oxides has enabled the synthesis of diverse P-doped π-conjugated molecules, demonstrating that activation of phosphorus centers by triflate significantly enhances their electrophilicity. Nevertheless, the utilization of inorganic phosphorus sources devoid of pre-existing C–P bonds has not yet been realized. Herein, we report a metal-free and direct phosphorus atom insertion into electron-rich π-systems using phosphorous acid (H$_3$PO$_3$) as a readily available and easily handled inorganic phosphorus source. Activation of H$_3$PO$_3$ with Tf$_2$O enables the formation of three C–P bonds in a single step, affording P-doped curved π-conjugated molecules. The resulting compounds exhibit pronounced emission arising from π−π* transitions enhanced by a multiple resonance effect, and display chiroptical properties due to their nonplanar geometries. This work establishes a new direct heteroatom insertion strategy, extending the concept previously demonstrated for boron to phosphorus, thereby expanding the chemical space of heteroatom-doped π-systems and providing a basis for future functional molecular design.

Introduction

The bottom-up synthesis of large polycyclic π-conjugated molecules yields structurally uniform nanographenes, which hold great potential for applications in nanoelectronics, optoelectronics, and spintronics.[1–4] Among these, curved nanographenes with three-dimensional (3D) structures have garnered attention due to their distinctive properties compared with planar π-systems, such as high solubility, chiroptical properties, and rich supramolecular chemistry.[5–9] Moreover, the
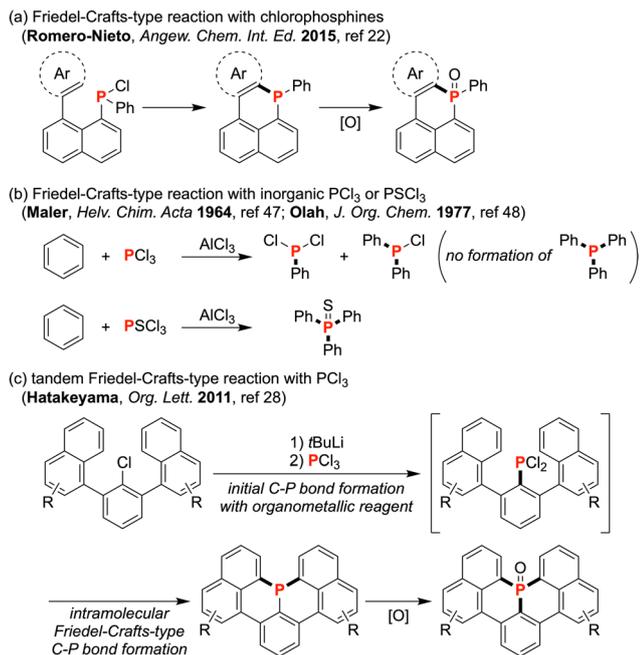
[a]Department of Molecular Engineering, Graduate School of Engineering, Kyoto University, Kyoto, 615-8510, Japan. E-mail: t-higa@scl.kyoto-u.ac.jp, imahori@scl.kyoto-u.ac.jp
[b]Institute for Chemical Research, Kyoto University, Kyoto 611-0011, Japan
[c]Institute for Integrated Cell-Material Sciences (iCeMS), Kyoto University, Kyoto, 606-8501, Japan
[d]Institute for Liberal Arts and Sciences (ILAS), Kyoto University, Kyoto, 606-8316, Japan

incorporation of heteroatoms into nanographenes has proven to be an effective strategy for modulating their structural, electronic, and magnetic properties without altering their frameworks.[10–13] In particular, phosphorus-doped (P-doped) polycyclic π-conjugated molecules have been extensively explored owing to their attractive properties such as highly electron-accepting ability and intense emission with high fluorescence quantum yields.[14–42] Furthermore, P-doped graphene has generated significant interest as a promising material for electrocatalysis, energy storage, sensing, and spintronics.[43–46]

In this context, introducing a phosphorus atom into a π-conjugated framework *via* the formation of three C–P bonds represents a direct and conceptually simple bottom-up approach to P-doped nanographenes and related functional π-systems. In general, Friedel–Crafts-type C–P bond formation using chlorophosphines is an effective method to synthesize P-doped π-conjugated molecules (Scheme 1a).[22–24] Nevertheless, the direct synthesis of triarylphosphine from phosphorus trichloride (PCl$_3$) through a triple C–P bond for-

2132 | *Org. Chem. Front.*, 2026, **13**, 2132–2142

This journal is © the Partner Organisations 2026

Scheme 1 Friedel–Crafts-type C–P bond formations from chlorophosphines.

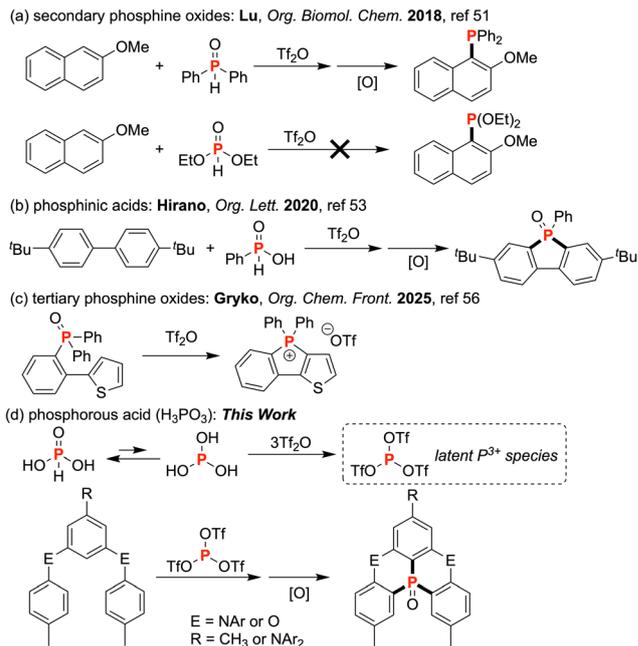**Scheme 2** Tf$_2$O-mediated Friedel–Crafts-type C–P bond formation reactions.

mation is not achieved, whereas the reaction of benzene with phosphorus sulfochloride (PSCl$_3$) affording triphenylphosphine sulfide has been reported as the only example of direct synthesis of triarylphosphine derivatives (Scheme 1b).[47–49] Therefore, a triple C–P bond formation directly from an inorganic phosphorus compound remains an extremely rare transformation. This challenge has been addressed by a tandem strategy involving the initial reaction of an organometallic reagent with PCl$_3$ to generate R–PCl$_2$ intermediates, which subsequently undergo intramolecular Friedel–Crafts-type C–P bond formation to complete the overall triple C–P bond formation (Scheme 1c).[28–31] Thus, achieving the direct formation of three C–P bonds using an inorganic phosphorus compound without employing any organometallic reagents, would represent a new strategy for the insertion of a phosphorus atom into a π-framework.

In recent years, several triflic anhydride (Tf$_2$O)-mediated Friedel–Crafts-type C–P bond formation reactions have been developed using organophosphorus oxides. For instance, the use of secondary phosphine oxides (R$_2$P(O)H) and phosphinic acids (RP(O)(OH)H) as phosphorus sources has enabled the synthesis of various π-conjugated compounds containing a phosphorus atom (Scheme 2a and b).[50–55] More recently, the reaction of tertiary phosphine oxides (R$_3$PO) with Tf$_2$O was also shown to afford the corresponding phosphonium salts (Scheme 2c).[56] These studies clearly demonstrate that the electrophilicity of the phosphorus center can be significantly enhanced through activation with triflate, thereby promoting electrophilic C–P bond formation under metal-free conditions. However, as reported by Lu and co-workers,[51] diethyl phosphite does not undergo C–P bond formation (Scheme 2a), indi-
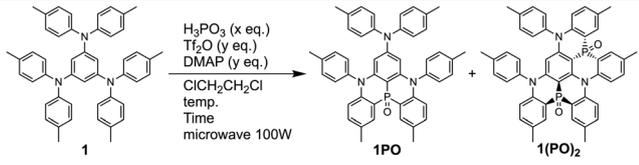
cating that the use of inorganic phosphorus compounds containing no pre-existing C–P bonds remains unachieved. Notably, the formation of a formal P(OTf)$_3$ species, corresponding to a phosphorus trication (P^{3+}), has been reported through the reaction of PCl$_3$ with silver triflate (AgOTf),[57] tempting us to develop the direct phosphorus atom insertion into π-conjugated frameworks via a P(OTf)$_3$-type intermediate by the activation with Tf$_2$O of phosphorous acid (H$_3$PO$_3$), an air-stable and readily available inorganic phosphorus compound. Herein, we report a direct phosphorus atom insertion into π-conjugated frameworks using H$_3$PO$_3$ as a readily available and easily handled inorganic phosphorus source. Activation of H$_3$PO$_3$ with Tf$_2$O enables the formation of three C–P bonds with electron-rich π-systems, affording a new class of P-doped polycyclic π-conjugated molecules (Scheme 2d).

Results and discussion

Phosphorus atom insertion into 1,3,5-tris(*N*,*N*-ditolylamino)-benzene

To validate our concept, we conducted the reaction of H$_3$PO$_3$ with 1,3,5-tris(*N*,*N*-ditolylamino)benzene **1** as a representative example. The microwave-assisted reaction of **1** (1 equiv.) with H$_3$PO$_3$ (5 equiv.) in the presence of Tf$_2$O (15 equiv.) and *N*,*N*-dimethylaminopyridine (DMAP) (15 equiv.) in 1,2-dichloroethane at 150 °C for 5 min using a microwave reactor yielded **1PO** with one P=O moiety as a sole product (43% yield) without oxidative treatment with H$_2$O$_2$, indicating that the initially formed P(III) species **1P** could spontaneously oxidize with residual Tf$_2$O *in situ* or with oxygen during workup under

Table 1 Reaction of 1,3,5-tris(*N,N*-ditolylamino)benzene **1** with H_3PO_3[a]

Entry	H_3PO_3/ eq.	Tf_2O/ eq.	Temp./ °C	Time/ min	$1PO$[b]/ %	$1(PO)_2$[b]/ %
1	5	15	150	5	43	0
2	5	5	150	5	0[c]	0
3	5	10	150	5	34	0
4	5	15	150	15	0	14
5	5	15	150	30	0	5
6	5	15	110	20	48	0
7	5	15	110	60	30	0
8[d]	5	15	110	20	0	0
9[e]	5	15	110	20	14[f]	0
10	10	30	150	15	0	13

[a] Reaction of **1** (0.075 mmol) in 1,2-dichloroethane (0.5 mL) was carried out under an argon atmosphere using a microwave reactor. [b] Isolated yield. [c] 75% of **1** was recovered. [d] The reaction was conducted without solvent. [e] The reaction was conducted in 1.5 mL of 1,2-dichloroethane. [f] 72% of **1** was recovered.

ambient atmosphere (Table 1, entry 1).[52] Although the reaction with 5 equivalents of Tf_2O and DMAP resulted in 75% recovery of **1** (entry 2), increasing the amount to 10 equivalents of Tf_2O and DMAP led to the formation of **1PO**, albeit in lower yield (entry 3). To investigate the role of Tf_2O and DMAP, we performed $^{31}P\{^1H\}$ NMR experiments in CD_3CN. Upon the treatment of H_3PO_3 with 3 equivalents of Tf_2O and DMAP, the distinct signal appeared at δ = 97 ppm, corresponding to the P^{3+} species, $[P(DMAP)_3][OTf]_3$ (δ = 102 ppm)[57] (Fig. S1). Using 2 equivalents also resulted in the formation of the P^{3+} species, whereas no such signal was observed with only 1 equivalent of Tf_2O and DMAP. These findings clearly indicate that the P^{3+} cation is a key reactive intermediate in the phosphorus atom insertion process. Nevertheless, mechanistic details of the C–P bond formation – whether stepwise or concerted – remain unsolved at this stage.

Then, we performed the reaction for 15 min, which produced **1(PO)₂** with two P=O moieties in 14% yield, while **1PO** was not detected (entry 4). Interestingly, only *anti*-isomer of **1(PO)₂** was obtained, even though two P=O moieties could lead to two isomers, namely, *anti*- and *syn*-isomers. The exclusive formation of *anti*-isomer implies that the *syn*-isomer is less stable, aligning with theoretical calculations (*vide infra*). Prolonging the reaction time led to a decreased yield of **1(PO)₂** (entry 5). In contrast, performing the reaction at a lower temperature (110 °C) afforded **1PO** in 48% yield (entry 6); however, **1(PO)₂** was not formed under these conditions, even with extended reaction times (entry 7). The reduced yield observed with longer reaction times may be attributed to the competitive decomposition pathways in the presence of Tf_2O (*vide infra*, Table S1). To evaluate the influence of the solvent volume, we examined the reaction under solvent-free con-

ditions as well as in a larger amount of 1,2-dichloroethane. Under solvent-free conditions, the reaction mixture generated an insoluble solid, and no P-doped product was obtained (entry 8). When the reaction was conducted in 1.5 mL of 1,2-dichloroethane, **1PO** was formed in 14% yield, accompanied by 72% recovery of **1** (entry 9). These results suggest that solvent is essential to maintain a homogeneous reaction environment, while a sufficiently high concentration is also required for efficient phosphorus atom insertion. In addition, increasing the amount of H_3PO_3 did not improve the yield of **1(PO)₂**, nor did it lead to formation of the product containing three P=O moieties (entry 10). The insertion of a third phosphorus atom may be hindered by structural constraints imposed by existing C–P bonds, as well as diminished reactivity resulting from the electron-withdrawing effects of the P=O groups. It is noted that using a conventional oil-bath heating instead of a microwave reactor required much longer reaction time and gave **1PO** and **1(PO)₂** in lower yields (Table S2).

The structures of **1PO** and **1(PO)₂** were unambiguously confirmed by single-crystal X-ray diffraction analysis (Fig. 1 and Fig. S2, Table S3). Following phosphorus insertion, **1PO** adopted a bowl-shaped conformation owing to a tetrahedral geometry of phosphorus atom. The unit cell for **1(PO)₂** contained two independent molecules within the asymmetric unit. Notably, **1(PO)₂** adopts the *anti*-configuration for the two P=O moieties and exhibits a hetero[4]helicene-like structure (rings A–D) (Fig. S2). Therefore, the insertion of multiple phosphorus atoms into arylamines proves to be an effective method toward P-doped helical π-systems.

We also attempted to reduce the P=O moieties of **1PO** and **1(PO)₂** to their corresponding P(III) species, **1P** and **1P₂**. However, the reaction of **1PO** or **1(PO)₂** with tetramethyldisiloxane (TMDS)[58] led to the complete recovery of **1PO** or **1(PO)₂**. Given that the σ^3,λ^3-phosphorus center embedded within electron-rich π-systems are often prone to oxidation under ambient conditions,[59–61] the observed resistance to reduction of the P=O moiety likely arises from the highly elec-
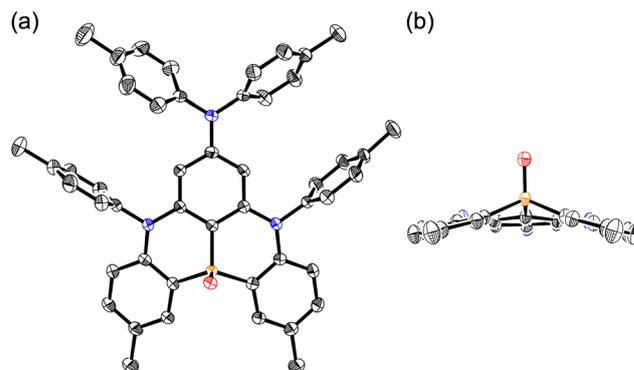

Fig. 1 X-Ray crystal structure of **1PO**: (a) top view and (b) side view. Thermal ellipsoids represent 50% probability. Solvent molecules and hydrogen atoms are omitted for clarity. In (b), *p*-tolyl groups are omitted for clarity.

tron-rich environment created by the presence of multiple nitrogen atoms.

Substrate scope

Using the conditions described in entry 6 of Table 1, we investigated the reactivity of various arylamines (Scheme 3). The reaction of compound **2**, bearing an electron-withdrawing CF_3 group, resulting in a 63% recovery of the starting material without formation of the corresponding P-doped product, consistent with the low reactivity of electron-deficient arenes toward Friedel–Crafts-type reactions. In contrast, compound **3**, featuring an electron-donating OMe group, provided **3PO** in

only 6% yield, with no detectable products containing two or three P=O moieties, despite the expected higher reactivity of **3** compared to **1**. To clarify this discrepancy, we conducted control experiments in the absence of H_3PO_3 (Table S1). Upon treatment with Tf_2O and DMAP, 93% of **2** was recovered, whereas only 15% of **3** remained. These results suggest that electron-donating substituents may facilitate competing decomposition pathways, thereby suppressing the formation of the desired P-doped product.

Additionally, the reaction of carbazolylbenzenes **4–6** afforded the corresponding P-doped products **4PO–6PO** in lower yield (4–36%) than **1PO**, which can be rationalized by
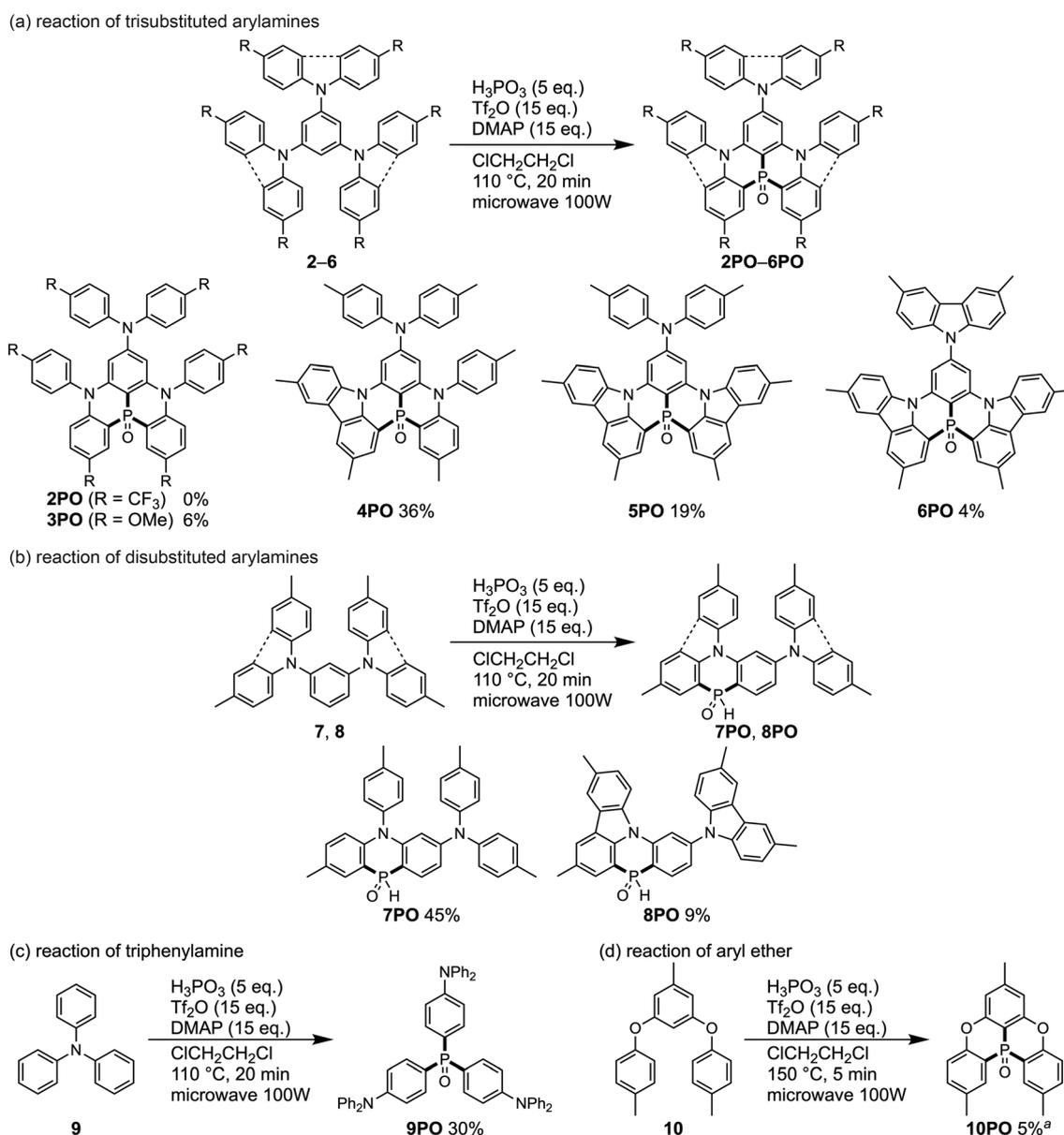
Scheme 3 Phosphorus atom insertion into arylamines and aryl ethers using H_3PO_3. Reaction conditions: arylamine (0.075 mmol), H_3PO_3 (0.38 mmol), Tf_2O (1.1 mmol), DMAP (1.1 mmol), 1,2-dichloroethane (0.5 mL); microwave irradiation at 110 °C for 20 min (100 W). [a] Modified conditions: compound **10** (0.15 mmol), H_3PO_3 (0.75 mmol), Tf_2O (2.3 mmol), DMAP (2.3 mmol), 1,2-dichloroethane (1.0 mL); microwave irradiation at 150 °C for 5 min (100 W).

the less electron-donating ability of carbazolyl moiety compared to the di(*p*-tolyl)amino moiety. In particular, the yield of **6PO** was only 4% under the standard conditions. To gain insight into the factors limiting the yield, we conducted the reaction of **6** with a shorter reaction time (10 min). In this experiment, **6PO** was obtained in 3% yield, while 47% of **6** was recovered. This result indicates that the low yield is likely attributed to competing decomposition pathways of either the substrate and/or the product during the reaction by Tf₂O (*vide infra*). Single-crystal X-ray diffraction analysis unambiguously confirmed the polycyclic structures of **4PO** and **5PO** (Fig. 2 and Table S3). The reaction of 1,3-disubstituted benzenes afforded the P(O)H-bridged products **7PO** and **8PO**, in which the phosphorus atom was selectively introduced at the *para*-position relative to the nitrogen atom on the central benzene ring. The presence of the P(O)H moiety in **7PO** and **8PO** suggests the formation of a P–OH intermediate during aqueous workup, which is subsequently converted to P(O)H. The formation of **9PO** from triphenylamine **9** further supports the enhanced reactivity at the *para*-position relative to the nitrogen atom, underscoring the importance of *para*-substitution in governing regioselectivity. Notably, we also demonstrated that this C–P bond-forming strategy is applicable to aryl ethers: the P-doped oxygen analogue **10PO** was successfully obtained from the corresponding aryl ether substrate. These findings demonstrate that this metal-free direct phosphorus atom insertion strategy can be applied to electron-rich π-systems, while the substrate scope is currently limited by the electronic requirements of the reaction. In addition, attempts to insert multiple phosphorus atoms into **3–6** by increasing the reaction temperature to 150 °C resulted in diminished product yields of **3PO–6PO** and no detectable formation of compounds bearing multiple P=O moieties. These outcomes can be attributed to competitive decomposition of **3** (*vide supra*) and the relatively lower electron-donating nature of compounds **4–6**, as reflected in their more positive oxidation potentials (0.44–0.77 V) compared to that of **1** (0.37 V) (Table S8, *vide infra*).

Photophysical properties

To investigate the effect of phosphorus atom on the photophysical properties of the products, we measured the UV/Vis
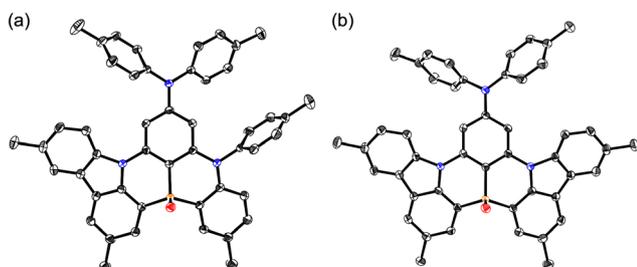

Fig. 2 X-Ray crystal structures of (a) **4PO** and (b) **5PO**. Thermal ellipsoids represent 50% probability. Solvent molecules and hydrogen atoms are omitted for clarity.

absorption and fluorescence spectra of **1**, **1PO**, and **1(PO)₂** in toluene (Fig. 3 and Table S4). The absorption maxima of **1PO** and **1(PO)₂** (λ_{abs} = 364 nm) are markedly red-shifted relative to that of **1** (λ_{abs} = 304 nm), which can be attributed to the π-extension facilitated by co-planarization of *p*-tolyl groups through C–P bond formation. In contrast, the fluorescence maxima of **1PO** (λ_{fl} = 388 nm) and **1(PO)₂** (λ_{fl} = 374 nm) are blue-shifted compared to that of **1** (λ_{fl} = 391 nm), reflecting the increased rigidity of their structures due to multiple C–P bonds, as further supported by their reduced Stokes shifts. Notably, **1PO** exhibits red-shifted absorption and fluorescence compared to those of P-centered triazatriangulene **11** (Fig. 4, λ_{abs} = 347 nm and λ_{fl} = 383 nm in CH₂Cl₂), which corresponds to a π–π* transition.[30] Given that the π-system of **1PO** is comparable to that of **11**, the observed red-shift in **1PO** suggests a significant contribution from intramolecular charge-transfer (ICT) interactions between the electron-deficient triarylphosphine oxide core and the electron-rich di(*p*-tolyl)amino substituent. Indeed, absorption and fluorescence spectra
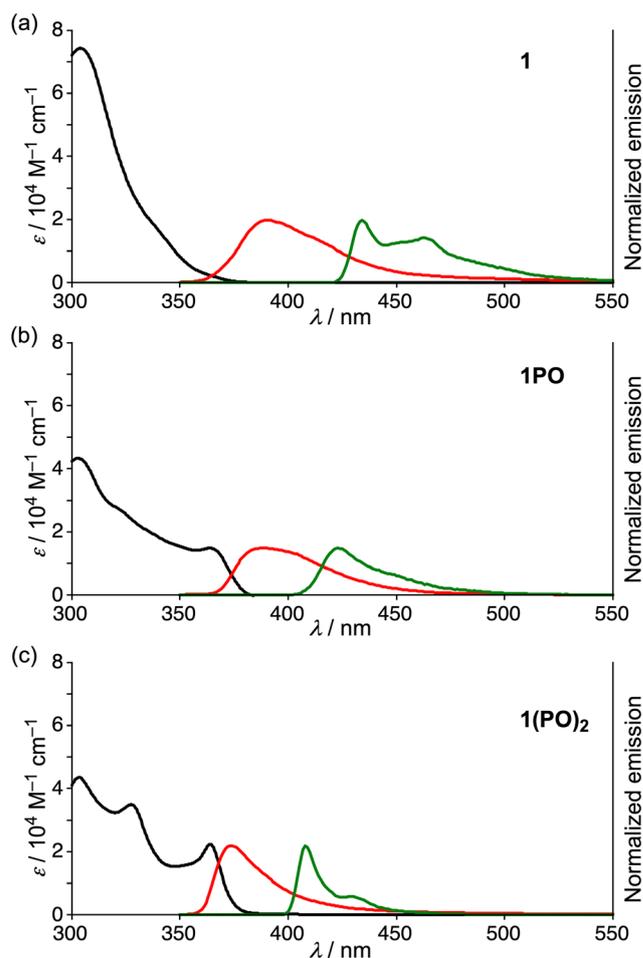

Fig. 3 UV/Vis absorption (black) and normalized fluorescence (red) spectra in toluene at room temperature, and normalized phosphorescence spectra (green) in 2-MeTHF at −190 °C (delay time: 0.05 ms) of (a) **1**, (b) **1PO**, and (c) **1(PO)₂**. The samples were excited at λ = 340 nm for both fluorescence and phosphorescence measurements.
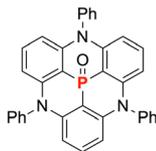
2136 | *Org. Chem. Front.*, 2026, **13**, 2132–2142

This journal is © the Partner Organisations 2026

Fig. 4 P-centered triazatriangulene **11**.

measured in various solvents revealed pronounced solvatochromic behavior, supporting the presence of ICT interaction (Fig. S3 and Table S5). In contrast, **1(PO)₂** exhibited no solvatochromism, indicating the absence of ICT character (Fig. S4). Although the fluorescence quantum yields (Φ_F) of **1PO** (0.11) and **1(PO)₂** (0.09) are higher than that of **1** (0.06), the fluorescence lifetimes (τ_F) were determined to be 0.7 ns and 0.5 ns for **1PO** and **1(PO)₂**, respectively, which are considerably shorter than that of **1** (1.4 ns) (Fig. S5). The radiative (k_r) and nonradiative (k_{nr}) rate constants are calculated from the Φ_F and τ_F values. The larger k_r values for **1PO** and **1(PO)₂** than that of **1** is ascribed to the effective π-delocalization over the co-planarized structure. On the other hand, the k_{nr} values for **1PO** and **1(PO)₂** increases with the number of P=O moieties. While the highly rigid structure tends to reduce non-radiative decays, the presence of phosphorus atoms may amplify the heavy atom effect, resulting in the lower Φ_F value for **1(PO)₂**. Moreover, **1PO** and **1(PO)₂** exhibit distinct phosphorescence maxima at 423 nm and 408 nm, respectively, in 2-MeTHF at −190 °C. From the fluorescence and phosphorescence maxima, we calculated the energy difference between the S_1 and T_1 states (ΔE_{ST}) to be approximately 0.28 eV for both **1PO** and **1(PO)₂**. The slightly smaller ΔE_{ST} values than that for **1** can be rationalized by multiple resonance effects of nitrogen and phosphorus atoms, reinforcing the potential of the phosphorus atom as an alternative to the boron atom in the concept of multiple resonance effects.[62–66] Nevertheless, preliminary photophysical studies for **1PO** and **1(PO)₂** revealed no evidence of thermally activated delayed fluorescence (TADF) (Fig. S6).

The P-doped products **3PO–6PO** exhibited photophysical properties similar to those of **1PO** (Fig. S7–S14 and Table S4). The higher Φ_F values observed for **4PO–6PO** compared to **1PO** can be attributed to their smaller k_{nr} values, which correlate with the enhanced structural rigidity imparted by the fused framework. Additionally, the smaller ΔE_{ST} values (approximately 0.3 eV) for **3PO–6PO**, relative to their parent compounds **3–6**, support the presence of a multiple resonance effect. In addition, the red-shifted absorption and fluorescence spectra of **7PO–10PO** upon phosphorus incorporation are also attributed to co-planarization of the molecular framework enabled by C–P bond formation.

Electrochemical properties

To investigate the electrochemical properties of **1**, **1PO**, and **1(PO)₂**, we performed cyclic voltammetry (CV) and differential pulse voltammetry (DPV) measurements (Fig. S15 and Table S6). The irreversible reduction peaks of **1PO** and **1(PO)₂** were observed at −2.92 and −2.77 V *versus* the ferrocene/ferrocenium couple (Fc/Fc⁺) in DMF, respectively, while no reduction peak was observed for **1** at potentials down to −3.5 V. The positive shift in the reduction potential (E_{red}) caused by the first P=O moiety should be larger than +0.5 V, whereas that by the second P=O moiety was only +0.15 V. The significantly larger effect induced by the first P=O moiety may be originated from the co-planarized π-system through C–P bond formation as well as the electron-accepting nature of the P=O moiety due to the effective σ⋆–π⋆ interaction. Additionally, **1PO** and **1(PO)₂** exhibited the irreversible oxidation peaks at +0.48 and +0.59 V in acetonitrile, which were positively shifted relative to that of **1** (+0.37 V). The positive shifts in oxidation potentials (E_{ox}) also reflect the electron-withdrawing nature of the P=O moieties. A similar trend was observed for compounds **3PO–10PO** (Fig. S16–S20 and Table S6), indicating that phosphorus atom insertion consistently influences the frontier molecular orbitals. Notably, the positive shifts in E_{red} values are substantially greater than that in E_{ox}, suggesting a more pronounced stabilization of the LUMO compared to the HOMO.

Density functional theory (DFT) calculations

To gain further insight into the structural and electronic properties of **1PO** and **1(PO)₂**, we performed DFT calculations at the B3LYP/6-31G(d,p) level. It is noteworthy that the *syn*-isomer of **1(PO)₂** is less stable than the *anti*-isomer by 30.7 kJ mol⁻¹, which is consistent with the selective formation of *anti*-isomer (Fig. S21). The HOMO of **1PO** is localized on the di(*p*-tolyl) amino group, while the HOMO−1 and LUMO are localized on the triarylphosphine skeleton. Notably, HOMO−1 exhibits significant orbital distribution on the nitrogen atoms and at the *ortho* and *para* positions relative to the phosphorus atom, whereas the LUMO shows extensive distributions on the phosphorus atom and at the *meta* positions (Fig. 5). These orbital distributions substantiate the multiple resonance effect in **1PO** and its relatively small ΔE_{ST} value. The energy levels of the HOMO and HOMO−1 are very close, indicating that these two molecular orbitals are nearly degenerated. Time-dependent
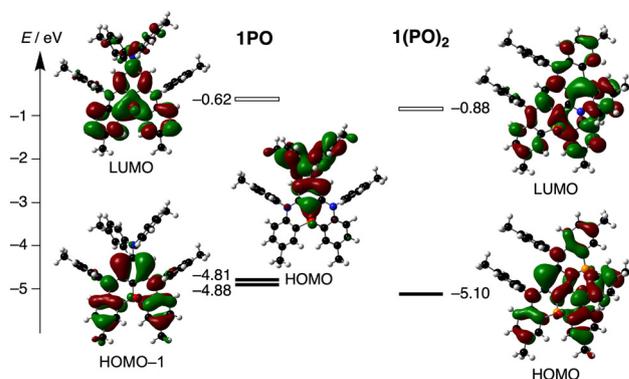

Fig. 5 Selected Kohn−Sham orbitals of **1PO** and **1(PO)₂** at the B3LYP/6-31G(d,p) level.

(TD) DFT calculations for **1PO** reveal two degenerated excitations (HOMO/LUMO and HOMO−1/LUMO) (Table S7), which is consistent with the mixing of a ICT transition (HOMO/LUMO transition) and π–π^* transition (HOMO−1/LUMO transition) on the lowest absorption band. Moreover, the TD-DFT calculations on the optimized geometry with the polarizable continuum model (PCM) using various solvents show good agreement with the solvatochromic behavior (*vide supra*) (Table S8). In contrast to **1PO**, the HOMO and LUMO of **1(PO)₂** are delocalized over the entire π-system, including the hetero[4]helicene-like structure. Moreover, the HOMO and LUMO of **1(PO)₂** exhibit suitable orbital distributions for the multiple resonance effect. Indeed, TD-DFT calculations for **1(PO)₂** indicate that the lowest excitation originates from the HOMO/LUMO transition (Table S7).

Chiroptical properties of 1(PO)₂ and 4PO

To investigate the chiroptical properties of **1(PO)₂** and **4PO**, which originate from nonplanar structures, the racemic mixtures were separated into their respective enantiomers using chiral HPLC (CHIRALPAK® IA) with CHCl₃ as the eluent (Fig. S22). The enantiomers exhibited mirror-image electronic circular dichroism (ECD) spectra with opposite cotton effects (Fig. 6). The absorption dissymmetry factors (g_{abs}) were deter-

mined to be 1.1×10^{-3} at 364 nm for **1(PO)₂** and 1.5×10^{-4} at 382 nm for **4PO**. Additionally, mirror-image circularly polarized luminescence (CPL) spectra were observed, with emission dissymmetry factors (g_{lum}) of 1.1×10^{-3} at 425 nm for **1(PO)₂** and 2.1×10^{-4} at 400 nm for **4PO**. It is noted that the peaks at 375 and 425 nm for **1(PO)₂** in the CPL spectra are attributable to emission from the monomeric and aggregated states, respectively, as the relative intensity (ΔI) at 425 nm increases compared to that at 375 nm under high concentrations (Fig. S23).[67] The g_{abs} value of **1(PO)₂** is comparable to that of the [4]helicene derivative **12** ($g_{abs} = 1.1 \times 10^{-3}$ at 434 nm),[68] indicating that the stabilization of the helical structure through the insertion of P=O moieties is advantageous for achieving chiroptical properties. To evaluate the stability of the enantiomers under thermal conditions, the isolated enantiomers of **1(PO)₂** and **4PO** were refluxed in toluene for 20 h, and subsequently analyzed by chiral HPLC. No significant decrease in enantiomeric purity was observed, indicating that racemization is negligible under these conditions (Fig. S24).

Conclusions

We have developed a new synthetic strategy for the direct insertion of phosphorus atoms into arylamines using H₃PO₃ as a readily available and easily handled inorganic phosphorus source. This method provides a straightforward and metal-free pathway to construct P-doped polycyclic π-conjugated systems through the formation of three C–P bonds in a single step. The products exhibit pronounced emission originates from π–π^* transitions enhanced by a multiple resonance effect, as supported by DFT calculations. Remarkably, the incorporation of phosphorus atoms emerges as a viable alternative to the B,N-doped π-systems realizing the multiple resonance effect. Additionally, **1(PO)₂** and **4PO** display unique chiroptical properties, stemming from their inherent chirality due to nonplanar configurations. This study demonstrates a new direct heteroatom insertion strategy that extends the concept of one-shot borylation previously established for boron[69–73] to phosphorus, thereby expanding the chemical space of heteroatom-doped π-materials. We anticipate that this direct phosphorus atom insertion strategy may serve as a basis for future developments toward more efficient and broadly applicable phosphorus atom insertion reactions, and for the design of functional P-doped π-systems, including curved polycyclic frameworks and related nanocarbon materials. Further exploration of phosphorus atom insertion into diverse π-frameworks, as well as efforts to expand the substrate scope, is currently underway in our laboratory.

$g_{abs} = 1.1 \times 10^{-3}$ at 434 nm
$g_{lum} = 1.1 \times 10^{-3}$ at 453 nm

12

Fig. 6 ECD and CPL (λ_{ex} = 300 nm) spectra of (a) **1(PO)₂** and (b) **4PO** in toluene. The sample concentrations for CPL measurements were 20 μM. The *g*-values of **12** were taken from ref. 68.

Author contributions

T. Higashino and H. Imahori conceived and designed this work. Y. Nishida and K. Ishida conducted the synthesis and characterization of the products. Y. Nishida performed spectro-
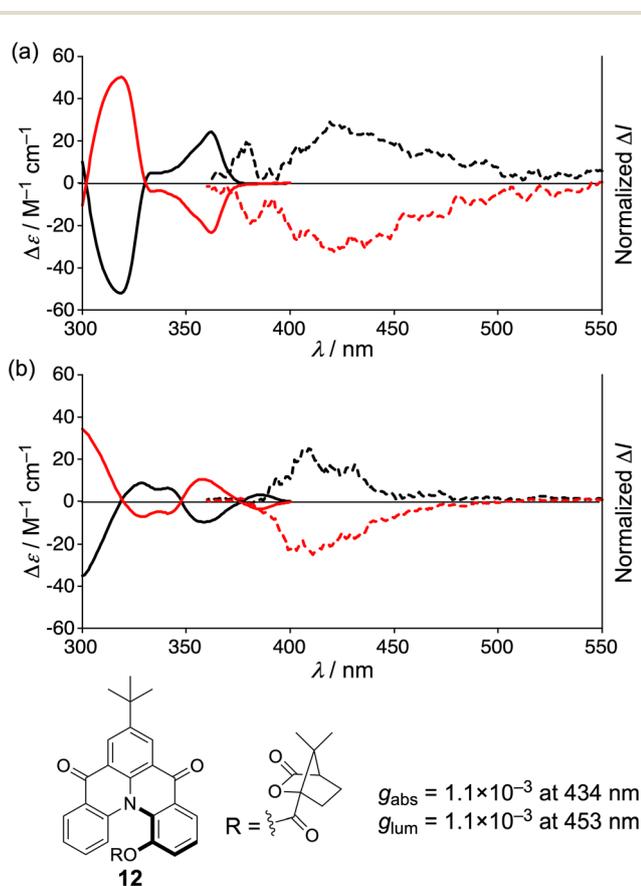
2138 | *Org. Chem. Front.*, 2026, **13**, 2132–2142

This journal is © the Partner Organisations 2026

scopic and electrochemical measurements. S. Kozaka, Y. Yasuda, and H. Kaji examined the TADF behavior. T. Higashino and H. Imahori co-wrote the manuscript.

Conflicts of interest

There are no conflicts to declare.

Data availability

The data supporting this article have been included as part of the supplementary information (SI). Supplementary information: experimental section, synthetic details, evaluation of reaction conditions, X-ray crystallographic details, optical and electrochemical properties, DFT calculations, chiroptical properties, HR-MS, and NMR spectra. See DOI: https://doi.org/10.1039/d5qo01428j.

Acknowledgements

References

1 A. Narita, X. Y. Wang, X. Feng and K. Müllen, New advances in nanographene chemistry, *Chem. Soc. Rev.*, 2015, **44**, 6616–6643.

2 Y. Segawa, H. Ito and K. Itami, Structurally uniform and atomically precise carbon nanostructures, *Nat. Rev. Mater.*, 2016, **1**, 15002.

3 R. S. K. Houtsma, J. De La Rie and M. Stöhr, Atomically precise graphene nanoribbons: interplay of structural and electronic properties, *Chem. Soc. Rev.*, 2021, **50**, 6541–6568.

4 Y. Gu, Z. Qiu and K. Müllen, Nanographenes and Graphene Nanoribbons as Multitalents of Present and Future Materials Science, *J. Am. Chem. Soc.*, 2022, **144**, 11499–11524.

5 I. R. Márquez, S. Castro-Fernández, A. Millán and A. G. Campaña, Synthesis of distorted nanographenes containing seven- and eight-membered carbocycles, *Chem. Commun.*, 2018, **54**, 6705–6718.

6 M. Saito, H. Shinokubo and H. Sakurai, Figuration of bowl-shaped π-conjugated molecules: properties and functions, *Mater. Chem. Front.*, 2018, **2**, 635–661.

7 S. H. Pun and Q. Miao, Toward Negatively Curved Carbons, *Acc. Chem. Res.*, 2018, **51**, 1630–1642.

8 T. Mori, Chiroptical Properties of Symmetric Double, Triple, and Multiple Helicenes, *Chem. Rev.*, 2021, **121**, 2373–2412.

9 H. V. Anderson, N. D. Gois and W. A. Chalifoux, New advances in chiral nanographene chemistry, *Org. Chem. Front.*, 2023, **10**, 4167–4197.

10 M. Stępień, E. Gońka, M. Żyła and N. Sprutta, Heterocyclic Nanographenes and Other Polycyclic Heteroaromatic Compounds: Synthetic Routes, Properties, and Applications, *Chem. Rev.*, 2017, **117**, 3479–3716.

11 X. Y. Wang, X. Yao, A. Narita and K. Müllen, Heteroatom-Doped Nanographenes with Structural Precision, *Acc. Chem. Res.*, 2019, **52**, 2491–2505.

12 M. Hirai, N. Tanaka, M. Sakai and S. Yamaguchi, Structurally Constrained Boron-, Nitrogen-, Silicon-, and Phosphorus-Centered Polycyclic π-Conjugated Systems, *Chem. Rev.*, 2019, **119**, 8291–8331.

13 A. Borissov, Y. K. Maurya, L. Moshniaha, W.-S. Wong, M. Żyła-Karwowska and M. Stępień, Recent Advances in Heterocyclic Nanographenes and Other Polycyclic Heteroaromatic Compounds, *Chem. Rev.*, 2022, **122**, 565–788.

14 M. P. Duffy, W. Delaunay, P.-A. Bouit and M. Hissler, π-Conjugated phospholes and their incorporation into devices: components with a great deal of potential, *Chem. Soc. Rev.*, 2016, **45**, 5296–5310.

15 P. Hibner-Kulicka, J. A. Joule, J. Skalik and P. Bałczewski, Recent studies of the synthesis, functionalization, optoelectronic properties and applications of dibenzophospholes, *RSC Adv.*, 2017, **7**, 9194–9236.

16 R. Szűcs, P. Bouit, L. Nyulászi and M. Hissler, Phosphorus–Containing Polycyclic Aromatic Hydrocarbons, *ChemPhysChem*, 2017, **18**, 2618–2630.

17 E. Regulska and C. Romero-Nieto, Highlights on π-systems based on six-membered phosphorus heterocycles, *Dalton Trans.*, 2018, **47**, 10344–10359.

18 T. A. Schaub, K. Padberg and M. Kivala, The Renaissance of Bridged Triarylphosphines: Towards Organophosphorus Molecular Bowls, *Chem. Lett.*, 2019, **48**, 1358–1367.

19 E. Regulska, P. Hindenberg and C. Romero-Nieto, From Phosphaphenalenes to Diphosphahexaarenes: An Overview of Linearly Fused Six-Membered Phosphorus Heterocycles, *Eur. J. Inorg. Chem.*, 2019, 1519–1528.

20 A. Heskia, T. Maris and J. D. Wuest, Phosphangulene: A Molecule for All Chemists, *Acc. Chem. Res.*, 2020, **53**, 2472–2482.

21 N. Asok, J. R. Gaffen and T. Baumgartner, Unique Phosphorus-Based Avenues for the Tuning of Functional Materials, *Acc. Chem. Res.*, 2023, **56**, 536–547.

22 C. Romero-Nieto, A. López-Andarias, C. Egler-Lucas, F. Gebert, J. Neus and O. Pilgram, Paving the Way to Novel Phosphorus–Based Architectures: A Noncatalyzed Protocol to Access Six–Membered Heterocycles, *Angew. Chem., Int. Ed.*, 2015, **54**, 15872–15875.

This journal is © the Partner Organisations 2026

Org. Chem. Front., 2026, **13**, 2132–2142 | **2139**

23 P. Hindenberg, M. Busch, A. Paul, M. Bernhardt, P. Gemessy, F. Rominger and C. Romero-Nieto, Diphosphahexaarenes as Highly Fluorescent and Stable Materials, *Angew. Chem., Int. Ed.*, 2018, **57**, 15157–15161.

24 P. Hindenberg, F. Rominger and C. Romero-Nieto, En Route Towards the Control of Luminescent, Optically–Active 3D Architectures, *Angew. Chem., Int. Ed.*, 2021, **60**, 766–773.

25 P. Hindenberg, A. Belyaev, F. Rominger, I. O. Koshevoy and C. Romero-Nieto, Two-Fold Intramolecular Phosphacyclization: From Fluorescent Diphosphapyrene Salts to Pentavalent Derivatives, *Org. Lett.*, 2022, **24**, 6391–6396.

26 E. Regulska, P. Hindenberg, A. Espineira-Gutierrez and C. Romero-Nieto, Synthesis, Post–Functionalization and Properties of Diphosphapentaarenes, *Chem. – Eur. J.*, 2023, **29**, e202202769.

27 R. Dadgaryeganeh, J. LeBlanc, E. Pradhan, D. Miao, A. Hussein, H. N. Hunter, T. Zeng, C. Romero-Nieto and T. Baumgartner, From flat to twisted – multifunctional phosphacyclic nanocarbons based on Vat Orange 3, *Chem. Sci.*, 2025, **16**, 3680–3692.

28 T. Hatakeyama, S. Hashimoto and M. Nakamura, Tandem Phospha-Friedel–Crafts Reaction toward Curved π-Conjugated Frameworks with a Phosphorus Ring Junction, *Org. Lett.*, 2011, **13**, 2130–2133.

29 S. Hashimoto, S. Nakatsuka, M. Nakamura and T. Hatakeyama, Construction of a Highly Distorted Benzene Ring in a Double Helicene, *Angew. Chem., Int. Ed.*, 2014, **53**, 14074–14076.

30 S. Nakatsuka, H. Gotoh, K. Kinoshita, N. Yasuda and T. Hatakeyama, Divergent Synthesis of Heteroatom–Centered 4,8,12–Triazatriangulenes, *Angew. Chem., Int. Ed.*, 2017, **56**, 5087–5090.

31 S. Nakatsuka, H. Gotoh, A. Kageyama, Y. Sasada, T. Ikuta and T. Hatakeyama, 5,9-Dioxa-13b-Oxophosphanaphtho[3,2,1-*de*]anthracenes Prepared by Tandem Phospha-Friedel–Crafts Reaction as Hole-/Exciton-Blocking Materials for OLEDs, *Organometallics*, 2017, **36**, 2622–2631.

32 S. Nakatsuka, Y. Watanabe, Y. Kamakura, S. Horike, D. Tanaka and T. Hatakeyama, Solvent–Vapor–Induced Reversible Single–Crystal–to–Single–Crystal Transformation of a Triphosphaazatriangulene–Based Metal–Organic Framework, *Angew. Chem., Int. Ed.*, 2020, **59**, 1435–1439.

33 A. Fukazawa, Y. Ichihashi, Y. Kosaka and S. Yamaguchi, Benzo[*b*]phosphole–Containing π–Electron Systems: Synthesis Based on an Intramolecular *trans*–Halophosphanylation and Some Insights into Their Properties, *Chem. – Asian J.*, 2009, **4**, 1729–1740.

34 C. Wang, A. Fukazawa, M. Taki, Y. Sato, T. Higashiyama and S. Yamaguchi, A Phosphole Oxide Based Fluorescent Dye with Exceptional Resistance to Photobleaching: A Practical Tool for Continuous Imaging in STED Microscopy, *Angew. Chem., Int. Ed.*, 2015, **54**, 15213–15217.

35 C. Wang, M. Taki, Y. Sato, A. Fukazawa, T. Higashiyama and S. Yamaguchi, Super-Photostable Phosphole-Based Dye for Multiple-Acquisition Stimulated Emission Depletion Imaging, *J. Am. Chem. Soc.*, 2017, **139**, 10374–10381.

36 R. A. Adler, C. Wang, A. Fukazawa and S. Yamaguchi, Tuning the Photophysical Properties of Photostable Benzo[*b*]phosphole *P*-Oxide-Based Fluorophores, *Inorg. Chem.*, 2017, **56**, 8718–8725.

37 T. Higashino, T. Yamada, T. Sakurai, S. Seki and H. Imahori, Fusing Porphyrins and Phospholes: Synthesis and Analysis of a Phosphorus-Containing Porphyrin, *Angew. Chem., Int. Ed.*, 2016, **55**, 12311–12315.

38 T. Higashino, K. Ishida, T. Satoh, Y. Matano and H. Imahori, Phosphole–Thiophene Hybrid: A Dual Role of Dithieno[3,4-*b*:3′,4′-*d*]phosphole as Electron Acceptor and Electron Donor, *J. Org. Chem.*, 2018, **83**, 3397–3402.

39 T. Higashino, K. Ishida, T. Sakurai, S. Seki, T. Konishi, K. Kamada, K. Kamada and H. Imahori, Pluripotent Features of Doubly Thiophene–Fused Benzodiphospholes as Organic Functional Materials, *Chem. – Eur. J.*, 2019, **25**, 6425–6438.

40 P.-A. Bouit, A. Escande, R. Szűcs, D. Szieberth, C. Lescop, L. Nyulászi, M. Hissler and R. Réau, Dibenzophosphapentaphenes: Exploiting P Chemistry for Gap Fine-Tuning and Coordination-Driven Assembly of Planar Polycyclic Aromatic Hydrocarbons, *J. Am. Chem. Soc.*, 2012, **134**, 6524–6527.

41 M. Yamamura, D. Hongo and T. Nabeshima, Twofold fused concave hosts containing two phosphorus atoms: modules for the sandwich-type encapsulation of fullerenes in variable cavities, *Chem. Sci.*, 2015, **6**, 6373–6378.

42 A. Tsurusaki, S. Tahara, M. Nakamura, H. Matsumoto and K. Kamikawa, Synthesis, Structures, and Properties of π–Extended Phosphindolizine Derivatives, *Chem. – Eur. J.*, 2023, **29**, e202203321.

43 S. Some, J. Kim, K. Lee, A. Kulkarni, Y. Yoon, S. Lee, T. Kim and H. Lee, Highly Air–Stable Phosphorus–Doped n–Type Graphene Field–Effect Transistors, *Adv. Mater.*, 2012, **24**, 5481–5486.

44 M. Latorre-Sánchez, A. Primo and H. García, P–Doped Graphene Obtained by Pyrolysis of Modified Alginate as a Photocatalyst for Hydrogen Generation from Water–Methanol Mixtures, *Angew. Chem., Int. Ed.*, 2013, **52**, 11813–11816.

45 R. Langer, P. Błoński, C. Hofer, P. Lazar, K. Mustonen, J. C. Meyer, T. Susi and M. Otyepka, Tailoring Electronic and Magnetic Properties of Graphene by Phosphorus Doping, *ACS Appl. Mater. Interfaces*, 2020, **12**, 34074–34085.

46 F. López-Urías, A. D. Martínez-Iniesta, A. Morelos-Gómez and E. Muñoz-Sandoval, Tuning the electronic and magnetic properties of graphene nanoribbons through phosphorus doping and functionalization, *Mater. Chem. Phys.*, 2021, **265**, 124450.

47 L. Maier, Organische Phosphorverbindungen. XI. Arylierung, von PSCl$_3$ in Gegenwart von Friedel–Crafts–Aktivatoren. Ein neues Verfahren zur Darstellung von Thiophosphoäure–dihalogeniden,

2140 | *Org. Chem. Front.*, 2026, **13**, 2132–2142

This journal is © the Partner Organisations 2026

Thiophosphinsäurehalogeniden und tertiären Phosphinsulfiden, *Helv. Chim. Acta*, 1964, **47**, 120–132.

48 G. A. Olah and D. Hehemann, Friedel-Crafts Type Preparation of Triphenylphosphine, *J. Org. Chem.*, 1977, **42**, 2190.

49 Z.-W. Wang and L.-S. Wang, Preparation of dichlorophenyl-phosphine via Friedel–Crafts reaction in ionic liquids, *Green Chem.*, 2003, **5**, 737–739.

50 H. Huang and J. Y. Kang, Triflic Anhydride (Tf$_2$O)-Activated Transformations of Amides, Sulfoxides and Phosphorus Oxides via Nucleophilic Trapping, *Synthesis*, 2022, 1157–1202.

51 T. Yuan, S. Huang, C. Cai and G. Lu, Metal-free electrophilic phosphination of electron-rich arenes, arenols and aromatic thiols with diarylphosphine oxides, *Org. Biomol. Chem.*, 2018, **16**, 30–33.

52 K. Nishimura, Y. Unoh, K. Hirano and M. Miura, Phosphenium–Cation–Mediated Formal Cycloaddition Approach to Benzophospholes, *Chem. – Eur. J.*, 2018, **24**, 13089–13092.

53 K. Nishimura, K. Hirano and M. Miura, Synthesis of Dibenzophospholes by Tf$_2$O-Mediated Intramolecular Phospha-Friedel–Crafts-Type Reaction, *Org. Lett.*, 2019, **21**, 1467–1470.

54 K. Nishimura, K. Hirano and M. Miura, Direct Synthesis of Dibenzophospholes from Biaryls by Double C–P Bond Formation via Phosphenium Dication Equivalents, *Org. Lett.*, 2020, **22**, 3185–3189.

55 K. Nishimura, S. Xu, Y. Nishii and K. Hirano, One-Step Synthesis of Benzophosphole Derivatives from Arylalkynes by Phosphenium-Dication-Mediated Sequential C–P/C–C Bond Forming Reaction, *Org. Lett.*, 2023, **25**, 1503–1508.

56 K. Górski, Ł. W. Ciszewski, A. Wrzosek, A. Szewczyk, A. L. Sobolewski and D. T. Gryko, An efficient method for the synthesis of π-expanded phosphonium salts, *Org. Chem. Front.*, 2025, **12**, 5484–5495.

57 S. S. Chitnis, A. P. M. Robertson, N. Burford, B. O. Patrick, R. McDonald and M. J. Ferguson, Bipyridine complexes of E^{3+} (E = P, As, Sb, Bi): strong Lewis acids, sources of E(OTf)$_3$ and synthons for E^I and E^V cations, *Chem. Sci.*, 2015, **6**, 6545–6555.

58 M. Berthod, A. Favre-Réguillon, J. Mohamad, G. Mignani, G. Docherty and M. Lemaire, A Catalytic Method for the Reduction of Secondary and Tertiary Phosphine Oxides, *Synlett*, 2007, 1545–1548.

59 T. Higashino and H. Imahori, Hybrid [5]Radialenes with Bispyrroloheteroles: New Electron-Donating Units, *Chem. – Eur. J.*, 2015, **21**, 13375–13381.

60 T. Higashino, I. Nishimura and H. Imahori, Phosphole–Fused Dehydropurpurins via Titanium–Mediated [2 + 2 + 1] Cyclization Strategy, *Chem. – Eur. J.*, 2019, **25**, 13816–13823.

61 T. Higashino, R. Minobe, T. Machino and H. Imahori, Unexpected cyclization of β-(hydroxymethyl)phosphole into 1-phospha-1,6a-dihydrophosphapentalene: a fused 1,3-butadiene-based luminophore, *Chem. Commun.*, 2025, **61**, 9420–9423.

62 H. Hirai, K. Nakajima, S. Nakatsuka, K. Shiren, J. Ni, S. Nomura, T. Ikuta and T. Hatakeyama, One–Step Borylation of 1,3–Diaryloxybenzenes Towards Efficient Materials for Organic Light–Emitting Diodes, *Angew. Chem., Int. Ed.*, 2015, **54**, 13581–13585.

63 T. Hatakeyama, K. Shiren, K. Nakajima, S. Nomura, S. Nakatsuka, K. Kinoshita, J. Ni, Y. Ono and T. Ikuta, Ultrapure Blue Thermally Activated Delayed Fluorescence Molecules: Efficient HOMO-LUMO Separation by the Multiple Resonance Effect, *Adv. Mater.*, 2016, **28**, 2777–2781.

64 M. Mamada, M. Hayakawa, J. Ochi and T. Hatakeyama, Organoboron-based multiple-resonance emitters: synthesis, structure–property correlations, and prospects, *Chem. Soc. Rev.*, 2024, **53**, 1624–1692.

65 H. Jiang, J. Jin and W. Wong, High–Performance Multi–Resonance Thermally Activated Delayed Fluorescence Emitters for Narrowband Organic Light–Emitting Diodes, *Adv. Funct. Mater.*, 2023, **33**, 2306880.

66 X.-F. Luo, X. Xiao and Y.-X. Zheng, Recent progress in multi-resonance thermally activated delayed fluorescence emitters with an efficient reverse intersystem crossing process, *Chem. Commun.*, 2024, **60**, 1089–1099.

67 S. Ito, K. Ikeda, S. Nakanishi, Y. Imai and M. Asami, Concentration-dependent circularly polarized luminescence (CPL) of chiral N,N′-dipyrenyldiamines: sign-inverted CPL switching between monomer and excimer regions under retention of the monomer emission for photoluminescence, *Chem. Commun.*, 2017, **53**, 6323–6326.

68 J. E. Field, G. Muller, J. P. Riehl and D. Venkataraman, Circularly Polarized Luminescence from Bridged Triarylamine Helicenes, *J. Am. Chem. Soc.*, 2003, **125**, 11808–11809.

69 K. Matsui, S. Oda, K. Yoshiura, K. Nakajima, N. Yasuda and T. Hatakeyama, One-Shot Multiple Borylation toward BN-Doped Nanographenes, *J. Am. Chem. Soc.*, 2018, **140**, 1195–1198.

70 S. Oda and T. Hatakeyama, Development of One-Shot/One-Pot Borylation Reactions toward Organoboron-Based Materials, *Bull. Chem. Soc. Jpn.*, 2021, **94**, 950–960.

71 A. Ikeno, M. Hayakawa, M. Sakai, Y. Tsutsui, S. Nakatsuka, S. Seki and T. Hatakeyama, π-Extended 9b-Boraphenalenes: Synthesis, Structure, and Physical Properties, *J. Am. Chem. Soc.*, 2024, **146**, 17084–17093.

72 L. Wu, Z. Huang, J. Miao, S. Wang, X. Li, N. Li, X. Cao and C. Yang, Orienting Group Directed Cascade Borylation for Efficient One–Shot Synthesis of 1,4-BN–Doped Polycyclic Aromatic Hydrocarbons as Narrowband Organic Emitters, *Angew. Chem., Int. Ed.*, 2024, **63**, e202402020.

73 X. Xiong, T. Chen, R. Walia, X. Fan, Y. Cheng, H. Wang, H. Wu, X. Chen, J. Yu, K. Wang and X. Zhang, Stepwise One–Shot Borylation Reactions for Intersecting DABNA Substructures Exhibiting Bright Yellow–Green Electroluminescence with EQE Beyond 40% and Mild Roll–Off, *Angew. Chem., Int. Ed.*, 2025, **64**, e202414882.

This journal is © the Partner Organisations 2026

Org. Chem. Front., 2026, **13**, 2132–2142 | **2141**

74 (*a*) CCDC 2361472: Experimental Crystal Structure Determination, 2026, DOI: **10.5517/ccdc.csd.cc2k89jp**; (*b*) CCDC 2361473: Experimental Crystal Structure Determination, 2026, DOI: **10.5517/ccdc.csd.cc2k89kq**;

(*c*) CCDC 2361474: Experimental Crystal Structure Determination, 2026, DOI: **10.5517/ccdc.csd.cc2k89lr**; (*d*) CCDC 2361475: Experimental Crystal Structure Determination, 2026, DOI: **10.5517/ccdc.csd.cc2k89ms**.

2142 | *Org. Chem. Front.*, 2026, **13**, 2132–2142

This journal is © the Partner Organisations 2026